Two-dimensional type-I intermittency

Chil-Min Kim* and Won-Ho Kye

National Creative Research Initiative Center for Controlling Optical Chaos, Pai-Chai University, Taejon 302-735, Korea
(Received 11 February 2000; published 21 February 2001)

The general structure of two-dimensional intermittency is discussed. The structure of channel and the trajectory in the return map are compared with those of one-dimensional intermittency and the scaling relations are obtained according to the trajectory. We illustrate the temporal behavior and scaling relations in a coupled map. The numerical results agree well with the theoretical predication of $\langle l \rangle \sim 1/\sqrt{\epsilon}$.

Intermittency is an occurrence of the signal that randomly alternates between almost regular (so-called laminar) periods and shorter chaotic bursts [1,2]. The phenomenon is frequently observed in real fluids, irregular reversals of the Earth's magnetic field, earthquakes, electronic circuits, etc. [3]. As it was considered to be one of the main routes to chaos, theoretical and experimental investigations followed to explore its scaling properties [4–6]. The scaling relation of the average laminar length depends not only on the structure of the local Poincaré map [2] but also on the reinjection probability distribution [6], since the laminar phase appears when a trajectory passes through the narrow channel between the local Poincaré map and the diagonal line in the return map and after escaping from the channel, the trajectory returns to it with a certain probability according to the global structure of the system. Also, the phenomenon shows an anomalous scaling relation [7,8] when noise is presented.

Recently, it was reported that intermittency is very important to the analysis of phase jump phenomena and the mysterious scalings near the synchronous regime [9]: For example, the investigation of type-I intermittency with noise enables us to analyze the phase jump phenomena and scaling in the coupled Rössler oscillators [7] and so does type-II intermittency with noise in the hyper-Rössler oscillators [8]. So studies of resolving the roots of phase synchronization were reinitiated in connection with intermittency. Despite all the rush, however, the problem is that all the studies are limited to low-dimensional chaotic systems because the most known intermittency is the low-dimensional phenomenon that can be described in a one-dimensional return map. To analyze phase synchronization of high-dimensional chaotic systems, studies of high-dimensional intermittency are required.

In this paper, as the first step for investigating high-dimensional intermittency, we introduce two-dimensional type-I intermittency [10] that occurs near the tangent bifurcation point like one-dimensional one, but which can be illustrated in a two-dimensional map that is not reducible to the one-dimensional return map [11]. We discuss the features of the system in comparison with those of one-dimensional intermittency in terms of scaling behaviors and the channel structure of the map.

The first-order difference equation in d dimension [12] is

$$\vec{x}_{n+1} = \vec{f}(\vec{x}_n), \qquad (1)$$

where $\vec{x}_n \in \mathbb{R}^d$ and $\mathbb{R}^d$ is the d-dimensional Euclidean vector space. The necessary condition for high-dimensional intermittency is $d \geq 2$. In order to set up the return map in high-dimension, we consider $(2d)$-dimensional vector space with $(\vec{x}_{n+p}, \vec{x}_n)$ by following the analogy in the one-dimensional return map, where $\vec{x}_{n+p}$ is the p-iterated image of $\vec{x}_n$ such that $\vec{x}_{n+p} = \vec{f}^{(p)}(\vec{x}_n)$ and p is the period of neighboring periodic orbit. The equation $\vec{x}_{n+p} = \vec{x}_n$ defines a d-dimensional diagonal hyper surface (DHS), which is a d-dimensional object embedded in $(2d)$-dimensional space.

It is difficult to visualize the geometrical shape of the high-dimensional return map unlike in one-dimension. Fortunately, however, in a two-dimensional system we are able to devise a suitable scheme to visualize the return map [13]. So we consider two-dimensional map such that $x_{n+1} = f(x_n, y_n)$, $y_{n+1} = g(x_n, y_n)$, which is locally defined near the bifurcation point. If we arrange two degrees of freedom, x_{n+1} and y_{n+1}, on the same axis we obtain a tractable three-dimensional view in terms of $(x_n, y_n, x_{n+1}, y_{n+1})$ coordinates and we call it a two-dimensional return map. The DHS is the two-dimensional surface embedded in $(x_n, y_n, x_{n+1}, y_{n+1})$ space that is defined by $x_{n+1} = x_n$ and $y_{n+1} = y_n$ (see Fig. 1) [14].

The gap between the DHS and the local map forms a channel and the system is in a state of the laminar phase when the trajectory passes the channel. The structure of the two-dimensional return map [13] can be clearly understood when we compare it with that of the one-dimensional one. The diagonal line in the one-dimensional return map becomes the DHS in the two-dimensional one. That is, the parabolic curve ($x_{n+1} = ax_n^2 + x_n + \epsilon$) in the one-dimensional return map becomes (because of the local property near the tangent bifurcation point) the parabolic surface in two-dimension such that

$$
\begin{aligned}
x_{n+1} &= a_1 x_n^2 + a_2 y_n^2 + a_3 x_n y_n + a_4 x_n + a_5 y_n + a_6, \\
y_{n+1} &= b_1 x_n^2 + b_2 y_n^2 + b_3 x_n y_n + b_4 x_n + b_5 y_n + b_6,
\end{aligned}
\qquad (2)
$$

where a_i and b_i are the arbitrary expansion coefficients. In the two-dimensional return map, there are two independent directions (x_n, y_n) and the next iteration point is determined by the sum of two evolution vectors.
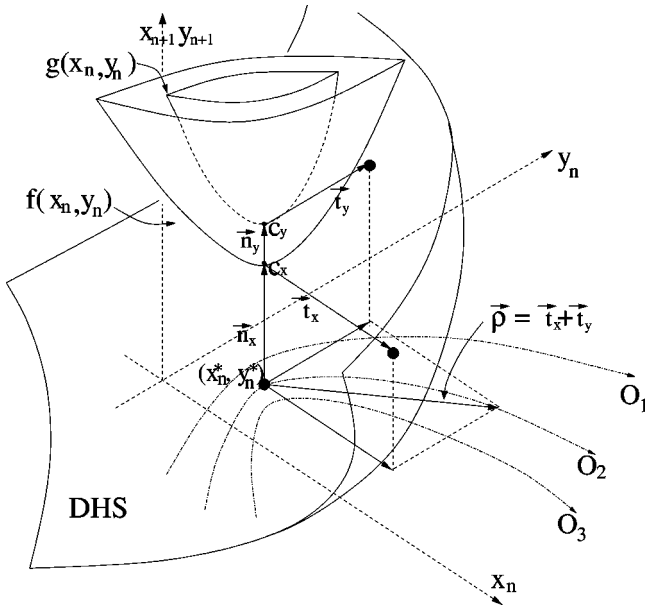
FIG. 1. The two-dimensional return map and the DHS.

Figure 1 shows a schematic view of our two-dimensional return map and its channels. According to the orbit (see O_1, O_2, and O_3 in Fig. 1) on the x_n-y_n plane the channel between the DHS and the local Poincaré map is differently formed as given in Fig. 1 and this causes the channel distribution. So in high-dimensional intermittency, one of the crucial factors that affect the laminar scaling is channel distribution function (CDF) $P(\epsilon)$.

The evolution procedure is as follows: at the initial point (x_n^*, y_n^*) we obtain the normal vectors $\vec{n}_x$ and $\vec{n}_y$ on the x_n-y_n plane and they contact at the points of $c_x = (x_n^*, y_n^*, x_{n+1}^*)$ and $c_y = (x_n^*, y_n^*, y_{n+1}^*)$, respectively, where $x_{n+1}^* = f(x_n^*, y_n^*)$ and $y_{n+1}^* = g(x_n^*, y_n^*)$. From those points we obtain the evolution vectors $\vec{t}_x$ and $\vec{t}_y$ after parallel stretching of the point to the DHS in the direction of x_n and y_n, respectively. Then the next iteration point is determined by the sum of two evolution vectors such that $\vec{\rho} = \vec{t}_x + \vec{t}_y$. The same procedure can be repeated to get time evolutions of a trajectory.

The intermittent behavior in two-dimension can be classified into three trajectories on the x_n-y_n plane [12]: (a) the *limit cycle* that shows a unique trajectory, (b) the *quasiperiodic* trajectory that uniformly fills a region and causes the uniform distribution of channel, and (c) the *chaotic* one whose channel gets a fractal structure by the chaotic passage. In case of the limit cycle, the channel structure is similar to that of one-dimensional type-I intermittency because the channel is unique. But for the others the channel structure is different from the conventional one because they suffer multichannel effects. Thus we see that the CDF plays a crucial role in the passage and the scaling relations of the average laminar length.

The above features are clearly illustrated when we consider the following two-dimensional map:
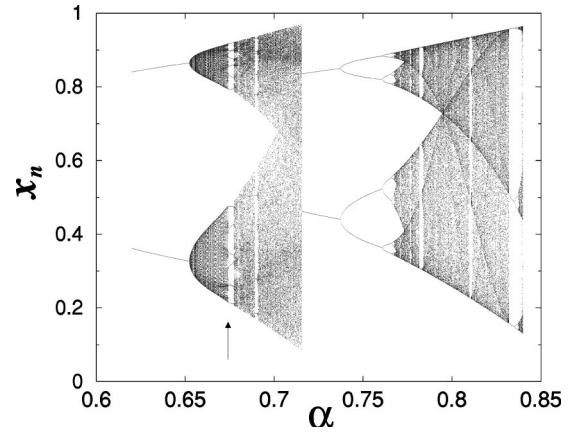

FIG. 2. The bifurcation diagram for $\beta = 0.5$. The inserted arrow points out the critical value of $\alpha_c = 0.674\,149\ldots$ for periodic orbit. (Note that the initial condition was not reset at each step of α to track an attractor.)

$$x_{n+1} = 4\alpha x_n(1-x_n) + \beta y_n(1-x_n),$$
$$y_{n+1} = 4\alpha y_n(1-y_n) + \beta x_n(1-y_n), \tag{3}$$

where α and β are parameters. The equations are two-dimensional extensions of the logistic map and can be considered as the mutually coupled system.

An example of bifurcation diagram is presented in Fig. 2 when $\beta = 0.5$. As α grows, the system develops to chaos via Hopf bifurcation $(0.6522\ldots < \alpha < 0.7172\ldots)$ and period doubling one $(0.7172\ldots \leq \alpha)$ [12]. It is interesting that the system spontaneously collapses to a one-dimensional system at $\alpha = 0.7172\ldots$. This phenomenon seems to be caused by the form of the couplings. In Eq. (3), if x_n and y_n are synchronized by chance in the overlapped chaotic band $(0.7017\ldots < \alpha < 0.7172\ldots)$ the coupled systems are completely synchronized and reduced to a one-dimensional logistic map.

The temporal behaviors of two-dimensional intermittency are given in Fig. 3 near the period-14 window at (a) $\alpha = 0.674\,103\ldots$, $\beta = 0.5$ and (b) $\alpha = 0.778\,2651\ldots$, $\beta = 0.3$ [15]. They are clearly distinguishable from those of the conventional intermittency. Figure 3(a) shows continuous in-
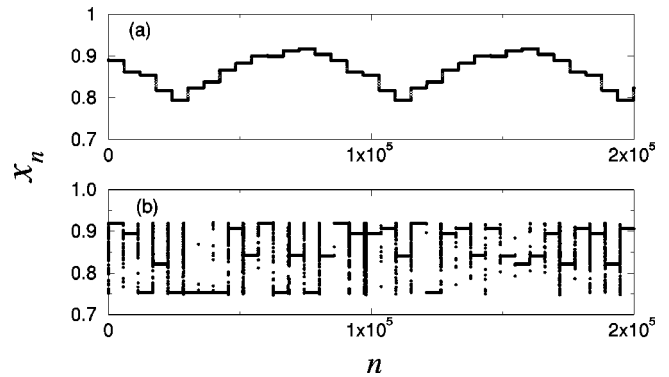

FIG. 3. The temporal behavior of two-dimensional intermittency near limit cycle (a) ($\alpha = 0.674\,103$, $\beta = 0.5$) and chaotic region (b) ($\alpha = 0.778\,2651$, $\beta = 0.3$).
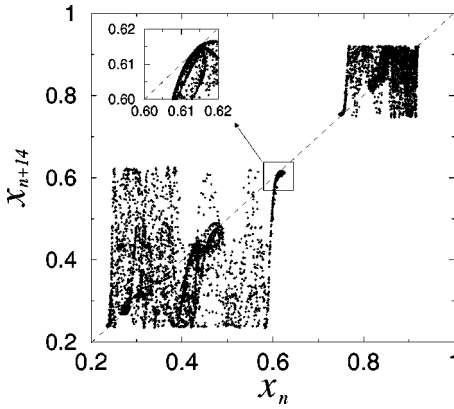
FIG. 4. The multichannel structure in the return map x_{n+14} versus x_n (at $\alpha = 0.778\,2651$, $\beta = 0.3$).

FIG. 5. The scaling of the laminar length on limit cycle (a) ($\alpha_c = 0.674\,149\,344\ldots$, $\beta_c = 0.5$) and chaotic region (b) ($\alpha_c = 0.778\,265\,11\ldots$, $\beta_c = 0.3$).

termittent jumps among laminar phases without chaotic bursts. And Fig. 3(b) shows irregular intermittent jumps with chaotic bursts. The reason for the difference is that while the former is the intermittency passing a limit cycle [case (a)], the latter is that passing a slightly different channel at each laminar phase (see Fig. 4).

What is observed above is clearly understood when we consider a two-dimensional return map on the parabolic surface $(x_n, y_n, x_{n+1}, y_{n+1})$. But we plot the return map on the (x_n, x_{n+1}) surface. The characteristics of two-dimensional intermittency are also revealed by the projection of the trajectory. We call this exotic one a multichannel structure to distinguish from the unique channel structure in one-dimensional intermittency [1–6].

Meanwhile, this multichannel structure caused by the orbits like O_1, O_2, O_3 in Fig. 1 is distinguished from the dispersed channel structure in the presence of noise [4,7], because the system follows a selected channel during the laminar phase. In the former, we can see a fractal-like channel structure in the return map, which is not the case in the latter. In addition, it was reported that the scaling relation of the laminar length for the latter is deformed such that $\langle l \rangle \sim \exp\{(1/D)|\epsilon|^{3/2}\}$ (where $\epsilon < 0$ and D is noise strength) by the effect of random noise [7,8]. Thus we emphasize that the conceptual difference between one- and high-dimensional intermittencies is the formation of multichannel structure.

The return map between x_{n+14} and x_n is presented in Fig. 4 when the trajectory is chaotic. In the inset figure, we can observe broad channel such as the effect of noise. But it is not caused by noise but by the multichannel structure, which is the key feature of two-dimensional intermittency. This is the irreducible return map mentioned above and the inset corresponds to the projected view of the parabolic surface in Eq. (2). The difference is obvious when we obtain the scaling relation.

The channel of this model is differently selected for each entrance point by following the perturbation of the coupled systems. These channel selections evoke the transversal deviation at the entrance point. On the contrary the reinjection process evokes the tangential one [6]. Near the tangent bifurcation point, the local Poincaré map can be modeled as
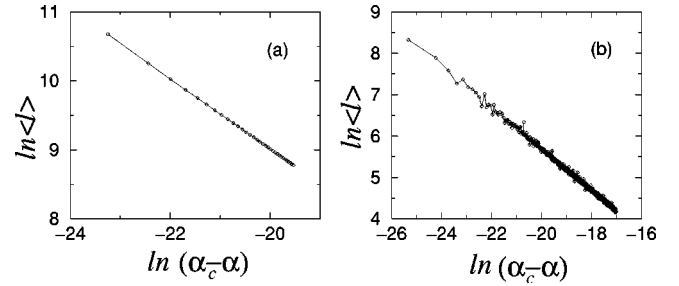
$$\dot{x} = ax^2 + \epsilon(y), \tag{4}$$

where a is the constant and $\epsilon(y)$ denotes the selected channel. It is assumed that in Eq. (4) an appropriate principal axis is taken in order to eliminate the cross term between x_n and y_n in Eq. (2).

x and y are injected into the laminar phase simultaneously and are in a state of the laminar phase. So if we adopt the simultaneous channel entrance approximation we can easily integrate Eq. (4) for a particular channel and obtain the laminar length scaling for a channel ϵ as follows [1,4,6]:

$$l(\epsilon, x_{in}) = \frac{1}{\sqrt{a\epsilon}}\left[\arctan\left(\sqrt{\frac{a}{\epsilon}}c \right) - \arctan\left(\sqrt{\frac{a}{\epsilon}}x_{in} \right) \right], \tag{5}$$

where x_{in} is the injection point and c is the escaping point of the laminar phase. The laminar scaling for a particular channel is the same as in one-dimensional case. However, the observable laminar length is the average in terms of the channel distribution function such that

$$\langle l \rangle = \int l(\epsilon, x_{in}) P(\epsilon) d\epsilon. \tag{6}$$

By taking the channel average we obtain the following scaling relation for each channel structure.

(a) *Limit cycle.* Near the quasiperiodic windows, we use the CDF such that $P(\epsilon) = \delta(\epsilon - \epsilon_0)$, since the trajectory is unique on the x_n-y_n plane and it forms a unique channel between the DHS and the local map. Then we obtain the following scaling law:

$$\langle l \rangle \sim \frac{1}{\sqrt{\epsilon_0}}. \tag{7}$$

(b) *Quasiperiodic orbit.* The CDF is uniform in this case such that $P(\epsilon) = 1/\Delta$ where Δ is a constant [6] and we consider the channel function such that $\epsilon(y) = ay^2 + \epsilon_0$ because of the uniform passage of y, where ϵ_0 is the nearest channel width. Then the laminar scaling is derived as follows:

$$\langle l \rangle = \int l(y, x_{in}) P(y) \frac{d\epsilon}{dy} dy \sim -\ln(\epsilon_0). \tag{8}$$

(c) *Chaotic region.* As shown in Fig. 4, the channel has the fractal structure. Because the fractal distribution is discrete, $P(\epsilon)$ can be represented by summation of delta functions and the laminar length is actually dominated by the longest one that comes from the nearest channel width ϵ_0 as

$$\langle l \rangle \sim \frac{1}{\sqrt{\epsilon_0}}. \tag{9}$$

Even though multiple channels are present, the scaling relation is invariant with that of one-dimensional type-I intermittency. If the channel distribution is continuous the scaling relation of the laminar length is drastically deformed as in the case of quasiperiodic orbit [see case (b). *Quasiperiodic orbits*]. Conversely, the scaling relation of $\langle l \rangle \sim 1/\sqrt{\epsilon_0}$ guarantees fractal distribution of the channels.

We simulate the laminar scaling near the period-14 window and present the results in Fig. 5. Near the chaotic and limit cycle regimes, the laminar scaling shows the scaling $\langle l \rangle \sim 1/\sqrt{\epsilon_0}$. The scaling relations confirm the previous analyses [Eqs. (7) and (9)]. We do not find an appropriate parameter range for quasiperiodic orbit in this model but expect to observe it in other systems. Once, there was a study on two-dimensional intermittency in area-preserving maps [16]. The author reported two different scalings but those were just two different representations of the case (a), which were caused by different trajectories traveling around the bifurcation point.

In conclusion, we have analyzed two-dimensional type-I intermittency. The return map has been extended to two-dimensional one to analyze the characteristics. Three kinds of possible intermittent time series have been discussed according to the trajectory on the x_n-y_n plane and their scaling relations were presented. The most crucial feature of two-dimensional intermittency is the formation of multichannel structure in the one-dimensional return map. This multichannel structure causes more complex temporal behaviors (in Fig. 3), but the scaling relation is invariant with that of one-dimensional type-I intermittency.

Note added. After the submission of the paper, we found independent study on two-dimensional intermittency of non-reducible coupled maps [17] that have different couplings from our model maps. They have rigorously analyzed the coupled maps in terms of renormalization group analysis without discussion of the channel structure. Their scaling agrees well with ours [Eq. (7)].

[1] P. Manneville and Y. Pomeau, Phys. Lett. **75A**, 1 (1979); Commun. Math. Phys. **74**, 189 (1990).

[2] E. Ott, *Chaos in Dynamical Systems* (Cambridge University Press, New York, 1993).

[3] D. J. Tritton, *Physical Fluid Dynamics* (Van Nostrand-Reinhold, New York, 1977).

[4] J. E. Hirsch, B. A. Huberman, and D. J. Scalapino, Phys. Rev. A **25**, 519 (1982).

[5] J. E. Hirsch, M. Nauenberg, and D. J. Scalapino, Phys. Lett. **87A**, 391 (1982); B. Hu and J. Rudnick, Phys. Rev. Lett. **48**, 1645 (1982); O. J. Kwon, C. M. Kim, E. K. Lee, and H. Lee, Phys. Rev. E **53**, 1253 (1996).

[6] C. M. Kim, O. J. Kwon, E. K. Lee, and H. Lee, Phys. Rev. Lett. **73**, 525 (1994); C. M. Kim, G. S. Yim, J. W. Ryu, and Y. J. Park, *ibid.* **80**, 5317 (1998).

[7] W. H. Kye and C. M. Kim, Phys. Rev. E (to be published); J. P. Crutchfield and J. D. Farmer, Phys. Rep. **92**, 45 (1982).

[8] I. B. Kim, W. H. Kye, S. Rim, Y. J. Park, and C. M. Kim (unpublished).

[9] M. G. Rosenblum, A. S. Pikovsky, and J. Kurths, Phys. Rev.

Lett. **76**, 1804 (1996); K. J. Lee, Y. Kwak, and T. K. Lim, *ibid.* **81**, 321 (1998).

[10] If the channel structure of the attractor is unfolded in $(x_n, y_n, x_{n+1}, y_{n+1})$ space, we call its temporal behavior near the channel two-dimensional intermittency.

[11] We say the return map is *reducible to one-dimension* when the channel structure can be represented by a simple curve in (x_{n+1}, x_n) space.

[12] S. H. Strogatz, *Nonlinear Dynamics and Chaos* (Perseus Books, New York, 1994).

[13] The two-dimensional return map is the portrait of an attractor in $(x_n, y_n, x_{n+1}, y_{n+1})$ space.

[14] The DHS consists of two planes that satisfy $x_{n+1} = x_n$ and $y_{n+1} = y_n$, but here to help the understanding of DHS, we visualize it as a simple surface in Fig. 1.

[15] Near other period windows we also observed similar temporal behaviors. Period-14 window is just an example.

[16] A. B. Zisook, Phys. Rev. A **25**, 2289 (1982).

[17] S. Y. Kim, Phys. Rev. E **59**, 2887 (1999).